Tribology Letters (2019) 67:51
https://doi.org/10.1007/s11249-019-1159-6

ORIGINAL PAPER

# Tribology of Selected Hard Coatings for Oil and Gas Applications Up to 450 °C

**Reza Gheisari**[1] · **Andreas A. Polycarpou**[1]

Received: 2 December 2018 / Accepted: 19 March 2019 / Published online: 4 April 2019


**Abstract**
Three different surface treatments, which are of interest to the oil and gas industry, and are commonly used for tribological applications at elevated temperatures, namely chromium carbide (CrC) coating, Ni–P coating, and boronized nickel alloy were investigated. In addition to different structural compositions, these surface treatments possess different surface topographies, which is of practical importance. Pin-on-disk experiments were conducted to measure their friction and wear performance against tungsten carbide. Experiments were carried out at room temperature and 450 °C using a specialized tribometer. Nanomechanical properties of the coatings were obtained at room and elevated temperatures. To investigate the physical and chemical changes that occurred during tribo-testing, scanning electron microscopy of the coatings' cross section, wear tracks, and wear debris were obtained. Energy-Dispersive X-ray Spectroscopy analysis revealed the changes in elemental composition of the coatings wear track after the experiments, which could affect their tribological performance. It was found that the intensity and composition of the generated oxides, changes in the mechanical properties of the surface materials with temperature, and the surface topographical characteristics affected the tribo-mechanism. Among the tested samples, boronized nickel alloy surface outperformed the coatings with lower friction coefficient and lower wear rate, especially at elevated temperature.

**Keywords** Oxidative wear · Adhesive wear · Boronizing · CrC coating · Ni–P coating

## 1 Introduction

Applying a thin hard coating on a relatively less wear resistant substrate has been proven beneficial to the tribological properties of contacting surfaces. Development of such thin layers started in the 1970s and were enhanced and evolved into today's commercial coatings [1]. Certain components that are required to operate at high temperature applications such as turbine components [2] and diesel engines [3] would experience premature catastrophic failures if not protected with specific hard coatings. Friction coefficient (COF), wear mechanisms, and wear rates are critical tribological parameters to measure, while investigating the coating performance at elevated temperatures. Also, tribochemistry plays an indispensable role at elevated temperatures [4]. Formation of different oxides could enhance or deteriorate the contact dynamics [5, 6]. Certain applications such as components used in artificial lifting systems, cavity pumps, and drilling tubes are a few examples where parts must endure high temperature sliding contacts in the oil and gas industry [7]. Other applications such as journal bearings in the impeller of an electrical submersible pump (ESP) are among machine components that are exposed to high temperature abrasive conditions [8]. To reduce the wear and friction in such components, applying hard coatings has the potential for excellent results. Nickel-based, chromium-based, and boron-based coatings are among the most common commercial hard coatings used for elevated temperature applications. This study investigates the tribological performance of one coating in each of the three categories at room temperature (RT) of 23 °C and elevated temperature of 450 °C.

Nickel-based coatings are suitable for elevated temperature applications such as jet engines and gas turbines [9]. High friction values observed with most hard coatings, including nickel-based coatings at elevated temperatures has been a challenge that was tackled by different strategies, including adding solid lubricants [10–12]. Such lubricants

✉ Andreas A. Polycarpou
apolycarpou@tamu.edu

[1] Department of Mechanical Engineering, Texas A&M University, College Station, TX, USA

deemed to be effective within a limited temperature range. Li and Xiong [13] conducted elevated temperature experiments (up to 600 °C) on nickel-based coatings with molybdenum disulfide and graphite as solid lubricants. Lee et al. [9] studied the effect of load on sliding wear of electrodeposited Zn–Ni coatings. Liu et al. reported a decreasing COF for self-lubricating nickel-based coatings at temperatures up to 600 °C. Other studies focused on nickel-based coatings performed at different testing conditions, however, the wear rates and COF generally remain within $1.0\times10^{-6}$–$5\times10^{-4}$ $mm^3/(N\ m)$ and 0.17–1.3, respectively, depending on lubricant additives and testing conditions including temperature [14–16].

Chromium nitride and titanium nitride tribological properties at elevated temperatures also received attention from researchers. In a study focused on CrCN, Polcar et al. [17] tested two different compositions of the same coating. Sudden increase of the COF from RT to 100 °C, followed by a steady-state region up to 400 °C, and then a sudden decrease in the COF was found to be the dominant behavior. In another study [18] to understand the effect of grain refinement on the tribological performance of coatings, vanadium was used as an additive to iron hard facing alloys. Polychronopoulou et al. [19] investigated the effect of adding Cu to Cr−N structure on its tribological performance at elevated temperatures up to 840 °C. Their analysis revealed that 3% Cu content was an optimal amount to enhance the wear and friction performance of Cr−N at 500 °C.

Boronizing and nitriding are surface treatments that could also enhance the tribological performance. Hardell and Prakash [20] tested plasma nitrided and surface coated tool steels at RT and 400 °C. It was shown that CrN coating provides significant improvement to its tribological performance at elevated temperatures. Taktak [21] studied the effect of boriding on the tribological performance of AISI 440C and 52100 bearing steels. Experiments were carried out from RT to 600 °C. It was concluded that at low temperatures, the dominant wear mechanism is brittle fracture and fine delamination, while at temperatures above 300 °C, mild oxidative wear is dominant. Considering a different application, Solzak and Polycarpou [22] tribotested WC/C and WC/C + DLC coatings relevant to air-conditioning and refrigeration compressors. Various extreme operating scenarios including elevated temperature conditions exhibited improvement in wear, friction, and scuffing susceptibility of the coated tribopairs.

From the aforementioned elevated temperature tribotesting, the importance of coating materials, testing conditions, and tribochemistry is evident. The present research aims at investigating three common coatings, most relevant to elevated temperature applications under severe operating conditions pertinent to oil and gas applications. Differences in mechanical, chemical, and topographical properties of the selected coatings provide a platform for comparison of the class of coatings each one represents.

## 2 Materials and Methods

### 2.1 High Temperature Tribometer (HTT) and Test Configuration

Figure 1a shows the high temperature tribometer (HTT) that was used to conduct the tribological experiments. The HTT is a versatile pin-on-disk apparatus for measuring in-situ friction and normal forces using a force transducer that is equipped with a feedback circuit to apply and maintain the pre-set normal force. The test chamber is comprised of a pin holder, a disk holder, and a three-layer glass enclosure, which is wired with heating elements. The inner surface of the outermost glass cylinder is coated with a thin gold coating to reduce radiation heat transfer. The HTT is capable of reaching chamber temperatures up to 1000 °C using heating elements made of FeCrAl alloy.

The test chamber is enclosed by a bell jar, which is a glass jar encased by a stainless-steel cylinder. The bell jar moves vertically to provide accessibility to the test chamber. The present experiments were conducted in open air/laboratory environment with a temperature of 21–24 °C and humidity of 35–50%. The HTT is capable of both unidirectional and oscillatory motions; rotating speeds from 0 to 1000 rpm and oscillation frequencies from 0 to 5 Hz. The force transducer records in-situ normal and friction forces up to 45 N. The ball-on-disk schematic configuration is shown in Fig. 1b, and Fig. 1c, d show images of a typical disk and pin (ball) used in this study. In all experiments, tungsten carbide-cobalt (WC–Co) balls with a diameter of 6.35 mm were used as pins. For brevity, it is referred to as tungsten carbide ball hereafter. Disks were all Dura bar 201 type 1 Ni-resist iron which has an average hardness of 160 HV and a tensile strength of 1700 MPa. It is an iron alloy with chemical composition of up to 3% carbon, 2.8% silicon, 1.5% manganese, 17.5% nickel, 7.5% copper, 2.5% chromium, and 0.12% sulfur. Disks have a 50.8 mm diameter and 5 mm thickness and are coated with different coatings. WC ball is chosen as a relatively harder and higher wear resistant counterface, which maintains its mechanical properties up to 600 °C [23]. This choice is in line with the focus of this work, which is to investigate the tribology of the selected hard coatings at elevated temperatures. Otherwise, the wear of the counterface would surpass the wear of the hard coatings and compromise the objectives of the study. Substrate i.e., Ni-resist alloy is a common material in electrical submersible pumps used in oil and gas applications [8]. No external lubricant was used at the contact, thus dry contact conditions were implemented in all tests. The pin is stationary and attached directly to the

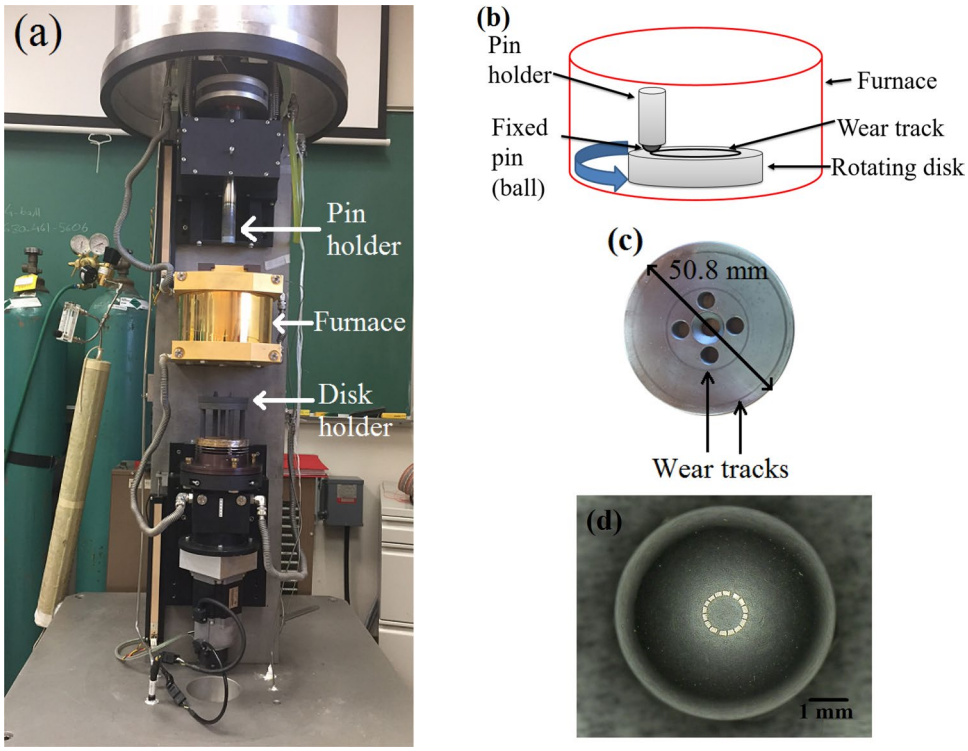


**Fig. 1** **a** High temperature tribometer, **b** schematic of the test chamber components, **c** typical used disk, and **d** spherical countersurface, 6.35 mm diameter

force transducer, while the disk is securely attached on a turntable that is connected to the electrical motor. Using a precise sliding mechanism, the diameter of the contact could be adjusted to the desired value.

## 2.2 Description of Surface Treatments

Three different hard coatings were selected based on their suitability for elevated temperature applications. Brief description of each surface coating and treatment are presented below:

(1) Chromium carbide coating ($Cr_xC_y$) is known to increase the wear resistance in elevated temperature applications. While it has lower wear resistance than WC, it is recommended as alternative for oxidative and corrosive environments. This coating is suitable for abrasion, fretting, and particle erosion environments. CrC was deposited on the substrate using thermal diffusion technique. The substrate is dipped into a molten salt bath at a temperature close to 1000 °C. The chemical reaction between the carbide forming elements and the substrate creates a metallurgical bonding with very high adhesion. The present coating treating time was 2 h which generated a chromium carbide layer with a thickness of 15 µm. This technique generates a relatively rough surface finish. XRD analysis of the coatings was obtained which demonstrates a prevalence of $Cr_3C_2$ and $Cr_7C_3$ phases [24].

(2) Boriding or boronizing (iron boride $Fe_xB_y$) is a thermochemical surface hardening process. This process could be carried out on ferrous and non-ferrous materials. The substrate is exposed to boron yielding material at high temperatures between 700 and 1000 °C. During this process the boron atoms diffuse into the substrate and create remarkably hard borides. The process can be done in solid, liquid, or gaseous mediums. The thickness of the boriding layer is determined primarily by the particle size of the powder used in boronizing, treatment time, treatment temperature, and substrate matrix. The dominant phases are FeB and $Fe_2B$ intermetallic ceramic borides in boronized stainless steel. Hardness and surface roughness of a boronized surface are affected by the treatment duration and temperature, and powder particle size.

(3) UltraKoat™ coating is a nickel-phosphorous (Ni–P) coating that is co-deposited with diamond-like submicron particles. Electroless nickel plating technique is a chemical plating process of nickel alloy in a heated solution. It is an autocatalytic chemical plating process applied at temperatures ranging from RT to 93 °C. UltraKoat has a melting temperature of 1030 °C and can be heat hardened to reach a hardness of 900 VHN. It is designed to provide corrosion and erosion resistance, along with a permanently lubricious contact surface. For consistency, this coating will be referred to as Ni–P coating. XRD analysis depicts the intense peaks of Ni, P, and NiP phases as dominant peaks in the coat-

ings structure [24]. Additional information regarding the deposition techniques of the coating is available in the literature [25–30].

### 2.3 Experimental Procedure

Before each experiment, the coated disks and WC balls were immersed in a bath of acetone and cleaned in an ultrasonic cleaner for 10 min. Then, they were rinsed with isopropanol and blown dry using a hot air blower. The WC ball was then placed in a pin holder and fastened using a setscrew. The disk was screwed onto the turntable that is connected to the motor shaft. The disk holder and pin holder were positioned in the furnace using the HTT control panel and the temperature was raised to the set temperature for each specific experiment, without making contact. Once the chamber reached the set temperature and stabilized, the pin and disk were brought into contact (at a pre-set normal load) and rotation was initiated and continued for 7500 cycles (1 h). In-situ normal and friction forces were measured using the force transducer and recorded on a computer. In all tests a normal force of 10 N was sustained at a sliding velocity of 0.2 m/s. All coatings were tested at 23 °C and 450 °C. To ascertain the repeatability of the obtained data, each test was conducted at least three times.

Once an experiment was completed, SEM and optical microscopy were carried out across the wear tracks and in an intact (or virgin) area. Wear track profiles were obtained across the wear track at three different locations, using a contact type profilometer. Assuming a uniform profile across the wear track, the wear volume could be readily obtained. Nanomecamical properties of the coatings were obtained using a Bruker TI Premier nanoinstrument. In addition, the Energy-Dispersive X-ray Spectroscopy (EDX) technique was employed on the wear tracks to investigate the chemical composition changes of the surfaces at the contact area due to the high contact pressure and temperature, and also on an intact location which was exposed to the elevated temperature during the test. Material transfer from one surface to the other was also revealed using the EDX technique.

## 3 Results and Discussion

### 3.1 Coating Properties

To characterize the coatings' mechanical and topographical properties, nanoindentation, 3D topography, and SEM analyses were employed. Specifically, hardness and reduced elastic modulus of the coatings were obtained using instrumented nanoindentation technique. 3D topography and relevant descriptive roughness parameters were obtained to determine the differences between the coatings; and SEM was implemented to measure the thickness of the coatings.

#### 3.1.1 Mechanical Properties

Hardness ($H$) and reduced elastic modulus ($Er$) of the boronized nickel alloy and Ni–P coatings at RT, 200 °C and 400 °C were obtained. Mechanical properties of the CrC coating were obtained by Zikin et al. [31] and was reported here. A diamond Berkovich indenter installed to a standard transducer was used. During high temperature experiments a flow of inert gas shielded the probe to prevent its degradation due to oxidation. To ascertain that the obtained data were not affected by substrate mechanical prosperities, the indentation depth was kept to less than 5% of the coating thickness. To take the effect of creep at high temperatures into consideration, a trapezoidal load function, as also suggested in the literature [32, 33], was used. In the present study a trapezoidal load function with 5-s loading and unloading segments and a two-second holding time was used. To obtain the optimum maximum load, a parametric study of the effect of load on the obtained nanomechanical properties was conducted. Figure 2 depicts the load–displacement data for the indentations conducted on the boronized nickel alloy sample at 200 °C with maximum loads of 2000 μN, 6000, μN, 8000 μN, and 10000 μN. To achieve a desired indentation depth (if too shallow then we may see skin or surface effects, and if too deep then we may experience substrate effects), the maximum load of 8000 μN was selected for all tests conducted on the boronized nickel alloy.

A similar procedure was conducted for the Ni–P coating. Due to lower hardness of the Ni–P coating, a maximum load of 4000 μN was selected as optimum load. For all nanoindentation experiments at different temperatures, several indentations were performed at different locations and the mean and standard deviations of the calculated values are shown in Table 1. The obtained data demonstrate the relatively small softening of the CrC coating at higher

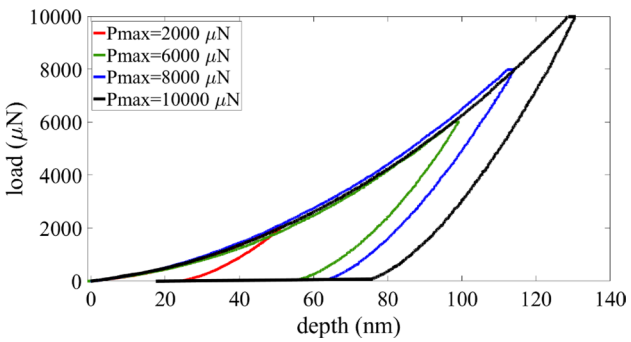


**Fig. 2** Load vs. displacement obtained for boronized nickel alloy coating at 200 °C

**Table 1** Nanomechanical properties of the coatings measured at RT, 200 °C, and 400 °C

| | RT | | 200 °C | | 400 °C | |
|---|---|---|---|---|---|---|
| | *Er* (GPa) | *H* (GPa) | *Er* (GPa) | *H* (GPa) | *Er* (GPa) | *H* (GPa) |
| CrC [31] | 360.0 ± 10.0 | 26.0 ± 1.5 | 370.0 ± 35 | 25.2 ± 2.0 | 381.0 ± 30 | 24.7 ± 3.0 |
| Boronized Ni alloy | 377.3 ± 17.7 | 28.6 ± 1.8 | 385.0 ± 12.2 | 25.7 ± 1.0 | 480.7 ± 19.1 | 24.8 ± 2.0 |
| Ni–P | 177.1 ± 12.2 | 7.83 ± 1.4 | 200.4 ± 9.2 | 6.4 ± 0.2 | 250.1 ± 15.0 | 2.33 ± 0.8 |

temperatures, while boronized Ni alloy is affected moderately, and Ni–P coating experiences the most notable degradation of hardness at 400 °C.

Nanomechanical properties of the WC–Co are available in the literature [34–37], even though a wide range of values are reported. An average hardness of 25 ± 5.0 GPa and reduced elastic modulus of 700 ± 50.0 GPA is assumed, based on the literature available for RT. At high temperatures, tungsten carbide is expected to sustain its mechanical properties up to 600 °C [23].

### 3.1.2 Topographical Properties

Figure 3a, c, e show cross section scanning electron microscopy (SEM) images of the coatings, as deposited on the substrate as well as their thickness. Figure 3b, d, f show the corresponding three-dimensional topographies. The roughness measurements were obtained using a KLA Tencor P-6 contact profilometer. The Ni–P coating has the smoothest surface while the CrC coating has the roughest surface. The roughness measurement area was 3000 µm × 3000 µm, and

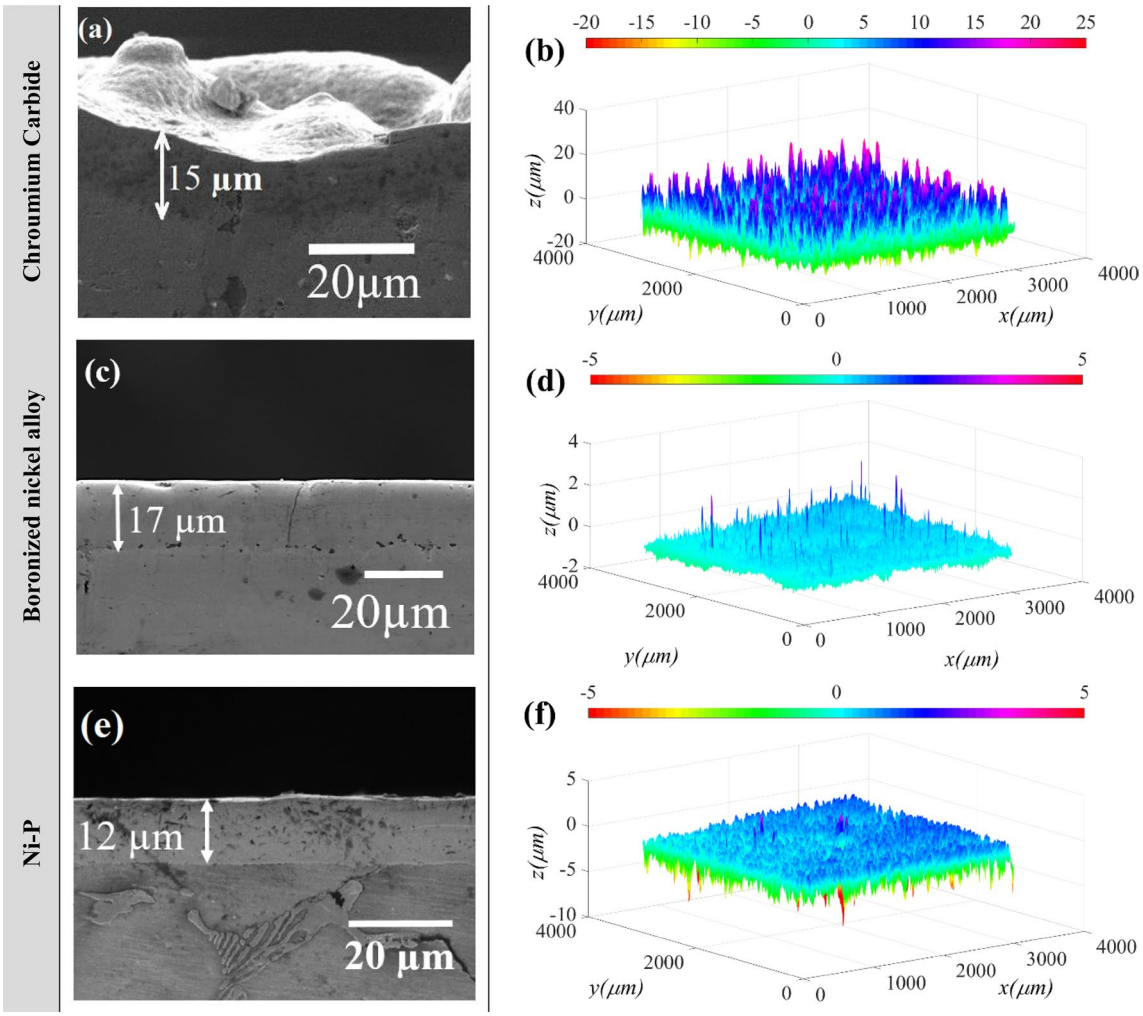


**Fig. 3** Cross section SEM and 3D topographies of **a, b** CrC; **c, d** boronized nickel alloy; **e, f** Ni–P coatings

the planar resolution is 1 μm in the x-direction and 10 μm in the y-direction.

Table 2 shows the calculated descriptive parameters of each coating topography as well as their measured thickness. While Sq and Sa represent the RMS and arithmetic average roughness of the topography, Sds indicates the density of summits per unit area of the surface. Summits are a subclass of the peaks of the topography. A peak is defined as a point higher than its adjacent 8 points. If a peak height exceeds 5% of the ten-point height of the surface then it represents summit. Additionally, summits must be separated by at least 1% of the minimum longitudinal or crosswise dimensions forming the 3D measurement area.

### 3.2 Tribological Results

In-situ friction and normal forces recorded during the experiments were used to obtain the COF as a function of time. Figure 4a depicts the COF for CrC, boronized nickel alloy and Ni–P coatings at 23 °C. For all cases, the COF transitions from an initial low value to a quasi-steady higher value. At the beginning of the experiments, within a run-in distance of 5–10 m, the COF values start at 0.1–0.3 and then surge to significantly higher values of 0.4–0.6. Then the COF values increase and do not reach a plateau until the very end of the tests such as CrC or boronized coatings. In addition, one could observe the increase in the oscillations of the COF as the tests continue, especially for Ni–P and CrC coatings. At the beginning of the tests, a point (Hertzian) contact occurs between the ball and the disk, and the mean Hertzian contact pressure for CrC, boronized and Ni–P coatings at RT were calculated at 2.23, 2.27, and 1.58 GPa. As the test proceeds, due to wear of the ball, and polishing of the contacting asperities on the coated disk, the nominal contact area increases. Providing that further sliding of the tribopairs results in their smoother surface finish, such topography evolution could promote and facilitate high frequency slip-stick behavior. This phenomenon is a possible explanation for the escalating standard deviation of the COF values as the test proceeds. In addition, debris generation and their subsequent cracking and crushing could contribute to the higher COF and its oscillation. Overall, Ni–P coating has the highest COF value and CrC and boronized nickel alloy exhibit lower COF values at RT.

Figure 4b depicts the changes in COF versus sliding distance for the substrate and tested coatings at 450 °C. Substrate data were used as a baseline for evaluating the performance of the coatings. An interesting observation in the COF behavior is the shortening of the time required for the quasi-steady state to emerge. The quasi-steady state term refers to the stable COF after the transient run-in period, if developed. At 450 °C the transition from run-in to quasi-steady state almost vanished and it matured quickly within 20–25 m of sliding. This behavior suggests the development of the contact dynamics which are discussed from a contact mechanics and chemical point-of-views in following sections.

A summary of the averaged COF values for the substrate and the different coatings tested at the two temperatures is shown in Fig. 5. Averaged values were obtained during the

**Table 2** Mechanical and roughness properties of the tested coatings and sphere

| Coating | $S_q$, RMS roughness (μm) | $S_a$, CLA roughness (μm) | $S_{ds}$, Density of summits (1/mm$^2$) | Thickness/depth (μm) |
|---|---|---|---|---|
| CrC | 4.78 | 3.58 | 1104 | 12–18 |
| Boronized nickel alloy | 0.83 | 0.60 | 1258 | 16–18 |
| Ni–P | 0.22 | 0.17 | 2362 | 12–15 |
| WC sphere | 0.18 | 0.12 | – | – |

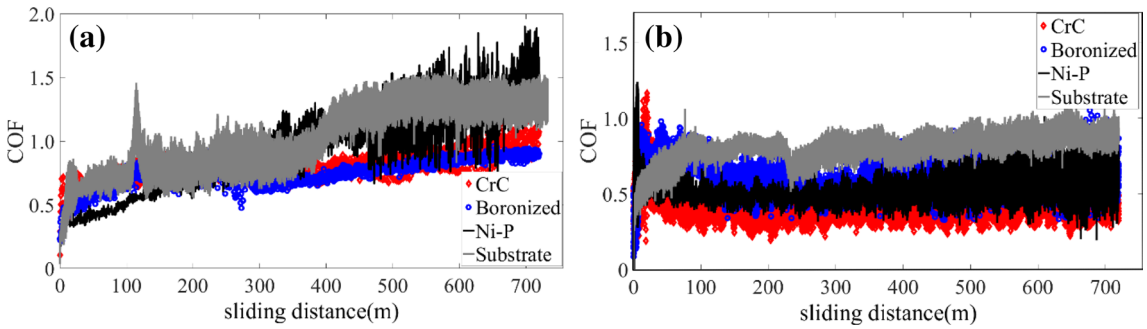


**Fig. 4** COF versus sliding distance for the coatings and the substrate at **a** RT (23 °C), **b** 450 °C

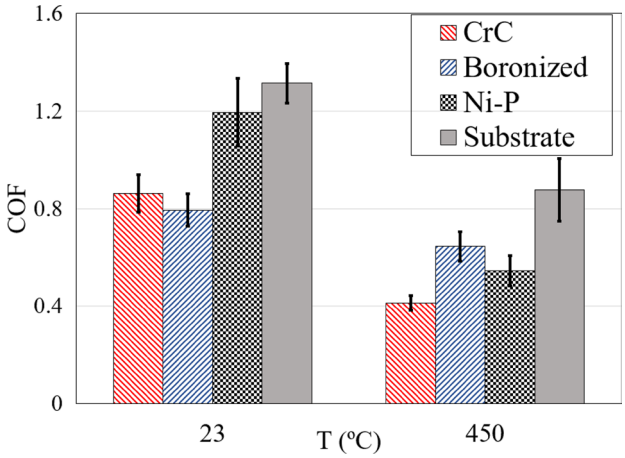


**Fig. 5** Average COF values of the coatings and substrate tested at RT (23 °C) and 450 °C. Error bars designate ± one standard deviation

last final 5 min of each experiment. The error bars designate the standard deviation of the COF values during this period. CrC and boronized coatings exhibit lower COF compared to the substrate at RT; However Ni–P shows similar COF to that of the substrate. At 450 °C all coatings show lower COF than the substrate. At RT, the boronized surface and CrC coating exhibit comparable COF, while Ni–P depicts a notably higher COF. Revisiting Table 1, note that the boronized surface and CrC coating have higher elastic modulus values than the Ni–P coating, which implies lower elastic deformation of asperities under identical loading. Moreover, the topography of the CrC coating and boronized nickel alloy (Fig. 3) shows rougher surfaces as well as fewer number of summits per unit area (Table 2). Both factors contribute to a smaller real contact area, which could explain the lower COF of CrC and boronized coatings. One could conclude the importance of the mechanical properties such as hardness and surface topography on the friction and wear performance of a hard coating at low temperature conditions.

The COF obtained for the substrate and all tested coatings exhibited a decreasing trend with temperature. This behavior and the obtained values of the tests presented in this study are similar to the data published in the literature for Ni–P coatings and boronized surfaces at elevated temperatures [38, 39]. With increasing temperature, the role of chemical composition of the surface treatments becomes more critical, especially when compared to its role at RT. The physical and chemical properties of the physio-chemical reaction products could alter the contact dynamics. Increasing the temperature to 450 °C leads to a drop in the COF values in all cases. A similar observation, namely a transition temperature at which a sharp reduction in COF occurs, was also reported for other coatings [4, 40, 41]. CrC and Ni–P coating experience sharp reduction in COF values of approximately 52% and 54% at 450 °C, while boronized coating sees a 19% reduction in the COF. Magnified changes in COF values reflect more intense changes of the contact conditions. That is, the COF behavior is related to the active wear mechanisms at the contact. Thus, understanding the wear mechanics will help determine the cause of the frictional changes.

To obtain the wear volume and wear rates, one needs to measure the wear track profiles, which are obtained from multiple profile scans across the wear tracks on the disks. In the present study, three scans of each wear track at three different locations were obtained. Figure 6 depicts typical wear scans for the substrate and the tested coatings at different temperatures. The length of the scans was set to 3 mm for all measurements with 1 µm longitudinal resolution and 10 nm height resolution. Double arrows were used to indicate the wear track width obtained on the disks at each temperature.

Substrate wear scans reveal a significant penetration depth for RT and 450 °C. Specifically, at elevated temperature the substantial increase in the worn material is visible. CrC coating's rough topography has a wide wear track at RT, which outweighs all other coatings at RT. However, the depth of the wear track is limited to truncated and flattened asperities, referred to as burnishing. The surface of the wear track after tests also shows a mildly polished and shiny finish. This wide polished area is because of the extremely hard CrC asperities which could grind the surface of the countersurface, the hard tungsten carbide ball, while enduring insubstantial wear. Boronized nickel alloy and Ni–P coatings however demonstrate a visible wear track for experiments conducted at RT; however not as wide as in the case of the CrC coating. For experiments conducted at elevated temperature the depth of the wear track increases for all cases, and in the case of Ni–P, the coating is almost penetrated. For a quantitative comparison of the intensity of the wear, details are provided in Table 3. These values were measured using SEM images of the wear tracks and were later verified with profilometric scans. At RT the depth of the wear track is related strongly to the hardness of the coating and its topography. Similar observation is applicable for the depth of the wear track at higher temperatures. However, degradation of the mechanical properties of the coating as a result of elevated temperature is a key factor in the more intense material removal from the sliding surface. Although CrC surface treatment provides the notably high hardness, it suffers a deeper and wider wear when compared to the boronized surface at 450 °C.

The Archard wear equation and related studies accentuate the role of hardness in wear, however the effect of the lubricous and/or protective oxide layers on the wear tracks, as well as the potential material transfer to the counter surface should also be considered. The last two mechanisms are known to be beneficial contributors to reduce wear and friction of coatings, especially at higher temperatures where the mechanical properties may degrade. While the width of

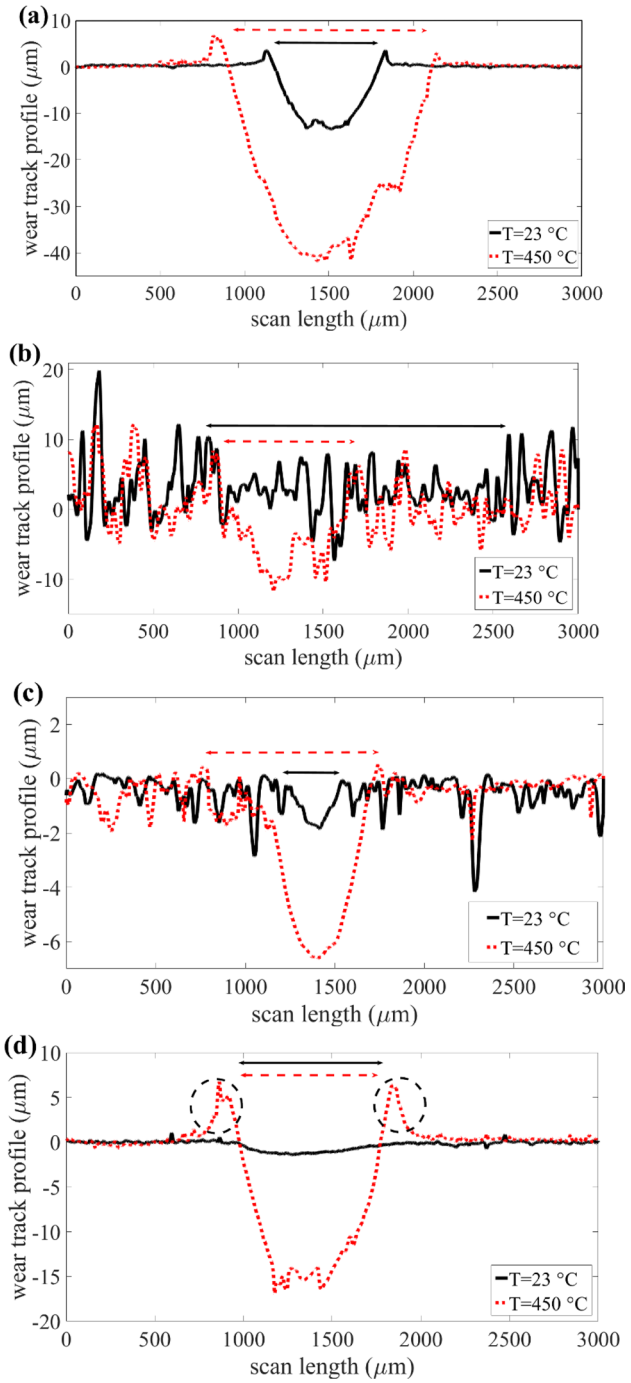


**Fig. 6** Wear profiles of **a** substrate, **b** CrC, **c** boronized nickel alloy and **d** Ni–P coatings at RT (23 °C) and 450 °C. Double arrows show the width of the wear track at each respective temperature. Dotted circles show material build-up. Note that the wear track profile scales (y-axes) are different

the wear track for the boronized nickel alloy increases with increase in temperature, it decreases in the case of CrC coating and remains almost constant for Ni–P coating. The wear track profile of the Ni–P coating depicts material build-up on both sides of the wear track, which is a known characteristic

**Table 3** Width and depth of wear tracks of the tested coatings

| | RT (23 °C) | | 450 °C | |
|---|---|---|---|---|
| | width (μm) | depth (μm) | width (μm) | depth (μm) |
| Substrate | 627 | 13.4 | 1210 | 41.7 |
| CrC | 2592 | 0[a] | 1713 | 11.8 |
| Boronized nickel alloy | 373 | 1.9 | 811 | 6.6 |
| Ni–P | 903 | 1.4 | 821 | 16.9 |

[a]Unmeasurable burnishing

of Ni–P coatings [42] and plays a role in reducing friction at higher temperatures. In this case, oxide particles on the build-up could provide a more lubricious contact condition which helps reduce the friction.

Based on the profilometric wear scans, we can calculate the volume of the coating and the substrate worn off as

$$V_{\text{worn}} = \int_{r_1}^{r_2} 2\pi.r.h.\mathrm{d}r = \sum 2\pi.r.h.\Delta r \tag{1}$$

where $r_1$ and $r_2$ are the inner and outer radii of the wear track, $h$ is the measured profilometric wear depth, and $\Delta r$ is the longitudinal resolution [43]. The mean value from three separate wear measurement estimations was used as the net wear volume, while the standard deviation was obtained as the error of the wear volume calculations. The wear rate was obtained using Eq. [2].

$$\dot{W} = \frac{V_{\text{worn}}}{F_{\text{N}} \times d} \tag{2}$$

where $\dot{W}$ is the calculated wear rate, $V_{\text{worn}}$ is the volume loss due to wear that is obtained by Eq. [1], $F_{\text{N}}$ is the applied normal load, and $d$ is the sliding distance. The wear profiles contribute to a better understanding of the wear mechanisms and contact severity, as well as obtaining the wear volume. Wear rates estimated using Eq. [2] for the substrate and the tested coatings at different temperatures are shown in Fig. 7. The inset depicts a zoom in scale of the wear rates of the coatings at RT. Ni–P performance escalates as the temperature increases, whereas boronized coating outperforms the other coatings and maintains a low wear rate even at elevated temperatures. All coatings exhibited remarkable improvement in wear performance when compared to the unprotected substrate, both at RT and 450 °C.

At RT, the wear mainly depends on the material mechanical properties and surface topography. Boronized coating with an average hardness of 28 GPa at RT and surface RMS roughness of 0.83 μm shows 1.5x and 2x lower wear rate than CrC and Ni–P coatings, respectively. CrC has a slightly

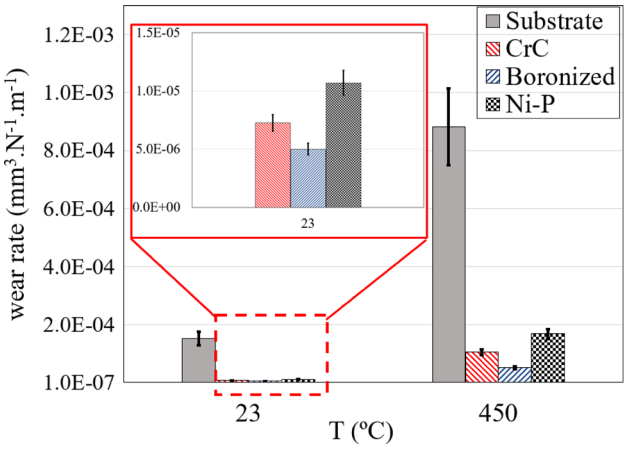


**Fig. 7** Average wear rates of the substrate and coatings tested at RT (23 °C) and 450 °C (calculated using Eq. [2])

lower hardness and Ni–P has the lowest roughness among the three tested coatings. Smoother surfaces imply a more uniform distribution of the load on the asperities that could bear the load without significant plastic deformation. However, with increasing operating temperature at the contact, other factors play significant role in the tribological performance of the interface too. These include the production of a protective oxide layer and its capability to generate a stable material transfer layer on the counter surface. These two mechanisms are functions of the material composition, surface roughness, contact load and sliding velocity among other parameters. Increasing the temperature to 450 °C can lead to softening of the coating materials [31, 44, 45]. The most visible effect of such changes in mechanical properties could be seen in the wear depth of the coatings as well as substrate. The wear rate of the substrate increases by a 6x factor. Those of Ni–P and CrC coatings increased by 15x while for the boronized coating the wear rate increased by 10x. Intensified material accumulation, squeezed on the sides of the wear track is visible for the Ni–P coating. The microstructural changes that lead to softening of the Ni coating at temperatures equal or higher than 400 °C have been widely studied [38, 46, 47]. Sudden increase of the wear track depth for the Ni–P coating at 450 °C, compared to wear tracks obtained for this coating at lower temperatures can be attributed to the softening of the coating (see Table 1).

### 3.3 SEM Analysis

SEM images of the wear tracks on the three coatings tested at RT are shown in Fig. 8a–c. Inset images show higher magnification images of the wear tracks. Figure 8d–f show SEM images of the tungsten carbide balls used against their respective coated disks. CrC coating wear tracks are covered with wear debris which initially may imply severe abrasive wear of the coating. However, a more careful investigation of the surfaces after cleaning the debris reveals mild polishing of the surface of the coatings as clearly shown in Fig. 6a. However, the wear debris is generated from harsh adhesive and possible abrasive wear of the tungsten carbide countersurface (Fig. 8d). Smooth surface finish of the ball is indicative of a dominant adhesive wear mechanism. The darker area of the inset image of Fig. 8a shows the polished asperities of the coating while the lower topography remained intact.

Boronized coating experiences adhesive wear and delamination that could be because of fatigue-induced cracking, as shown in the inset of Fig. 8b. The dominant wear mechanism of the countersurface ball seems to be adhesive wear, which resulted in polishing and plastic deformation in the form of material pull-out from the contact. The relatively higher hardness and smoother topography of the boronized coating seems to be responsible for a narrower wear scar on the ball, which has almost half the diameter of the wear scar on the ball slid against CrC coating (Fig. 8d).

Ni–P coating has the lowest hardness and RMS roughness. Both factors could attribute to easier plastic deformation of the surface and stronger adhesive wear. Polished asperities of the Ni–P coating shown in the inset of Fig. 8c depict the slight polishing of the surface while the lower topography remained intact. Mild adhesive wear is the dominant wear mechanisms in the Ni–P coatings sliding against stainless steel at RT, consequently the wear track exhibits a smooth finish [48]. Ni–P coating wear rate is 1.5x the wear rate of CrC coating, despite the fact that its hardness is almost 3x lower than that of CrC coating. However, the Ni–P coating has a remarkably lower surface roughness, which is the key contributor which compensates the lower hardness. This finding supports the importance of surface roughness in determining the wear rate of hard coatings at low temperatures. Consequently, the boronized coating which benefits both from high hardness and smooth surface experiences the lowest wear and imposes lower damage to the countersurface.

Interface temperature plays an indispensable role in the tribodynamics of contacting interfaces. Softening of the coating materials translates to lower resistance of the asperities towards elastic or plastic deformation. Lower hardness could facilitate the ploughing and removing of the materials from the sliding contact. In addition, high operating temperatures could initiate or accelerate chemical reactions of the coating materials with the environment which could directly or indirectly affect the tribodynamics. Formation of boric acids on the wear track as a result of the chemical reaction between boron oxide and ambient humidity is recognized as a self-lubricating mechanism that contributes to the reduction of the COF at higher temperatures for boronized surfaces [49–51]. Increasing the temperature to 450 °C results

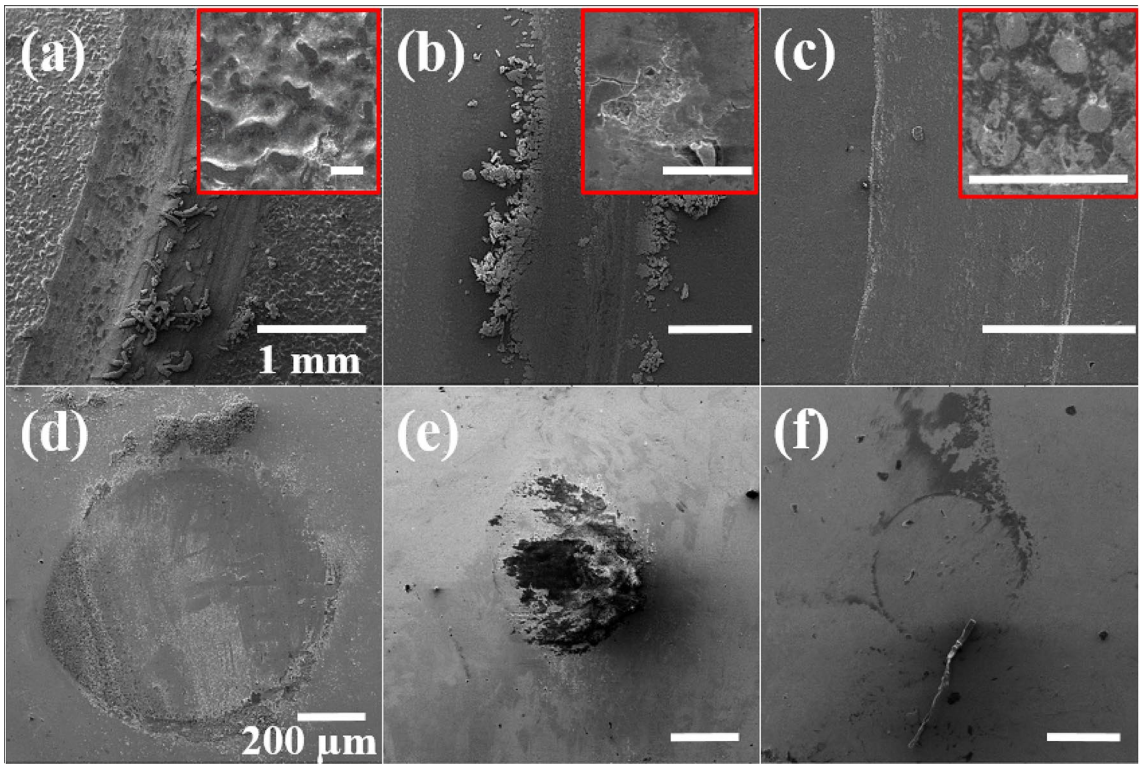


**Fig. 8** SEM images of the wear tracks on disks (**a, b, c**), and corresponding tungsten carbide balls (**d, e, f**) tested at RT. **a, d** CrC coating; **b, e** boronized coating; **c, f** Ni–P coating. Scale bars show the same length in each row. Scale bar in the insets is 50 µm

in the reaction of the coating's elements with the oxygen that is abundant in the ambient air and production of several oxides. Oxidation could promote intensified material removal of the surface due to changes in material properties and the grain reconstruction of the surface [17]. Significant changes in the microstructure of the coatings at elevated temperatures, especially Ni–P coatings, were reported in the literature [38, 46, 47]. In addition, oxide particles could interact as a third body abrasives and exacerbate wear. Nonetheless, providing adequate adhesion between the oxide layer and the sliding counterface, it facilitates a self-lubricating mechanism. This layer could reduce the friction and wear of the contact.

SEM images of the CrC, boronized nickel alloy, and Ni–P coatings at 450 °C at two different magnifications are shown in Fig. 9. Increasing the temperature to 450 °C affects the wear tracks visibly. In case of the CrC coating, there is significant increase in the wear depth as measured by surface profilometry. In addition, increasing the temperature to 450 °C causes the emergence of a vivid wear track with readily distinguishable darker interface as shown in Fig. 9a. At higher temperature a tribofilm called glaze layer is formed on the wear track which could help reduce the wear and friction of the surface [42]. This tribofilm consists of fractured and oxidized wear debris whose generation is normally accelerated and intensified as the temperature increases (Fig. 9d). The wear mechanisms at high temperatures are typically fatigue-induced delamination due to cyclic loading and plastic deformation, such as ploughing. This fully developed uniform layer could reduce the friction and help protect the exposed material from excessive oxidation which could deteriorate the delamination of the coating. Figure 9d depicts the delamination of the glaze layer under high contact pressure. Revisiting Fig. 8a, the accentuated effect of surface roughness at RT is alleviated at high temperature due to rapid changes in the surface topography with packing and molding of the wear debris.

The boronized coating shows a more uniform surface as shown in Fig. 9b. The dominant wear mechanism of the boronized coating at elevated temperature seems to be adhesive wear. Delamination of the boronized surface occurred due to adhesion or fatigue resulted from cyclic loadings (Fig. 9e). Boronized nickel alloy surface maintains its mechanical integrity and experienced minimal wear as demonstrated in Table 1, and Fig. 7 respectively.

In the case of Ni–P coating, severe material removal in the form of material lumps pulled out of the wear track is visible in Fig. 9c. Material build-up on the sides of the wear track which was shown using profilometry is also denoted.

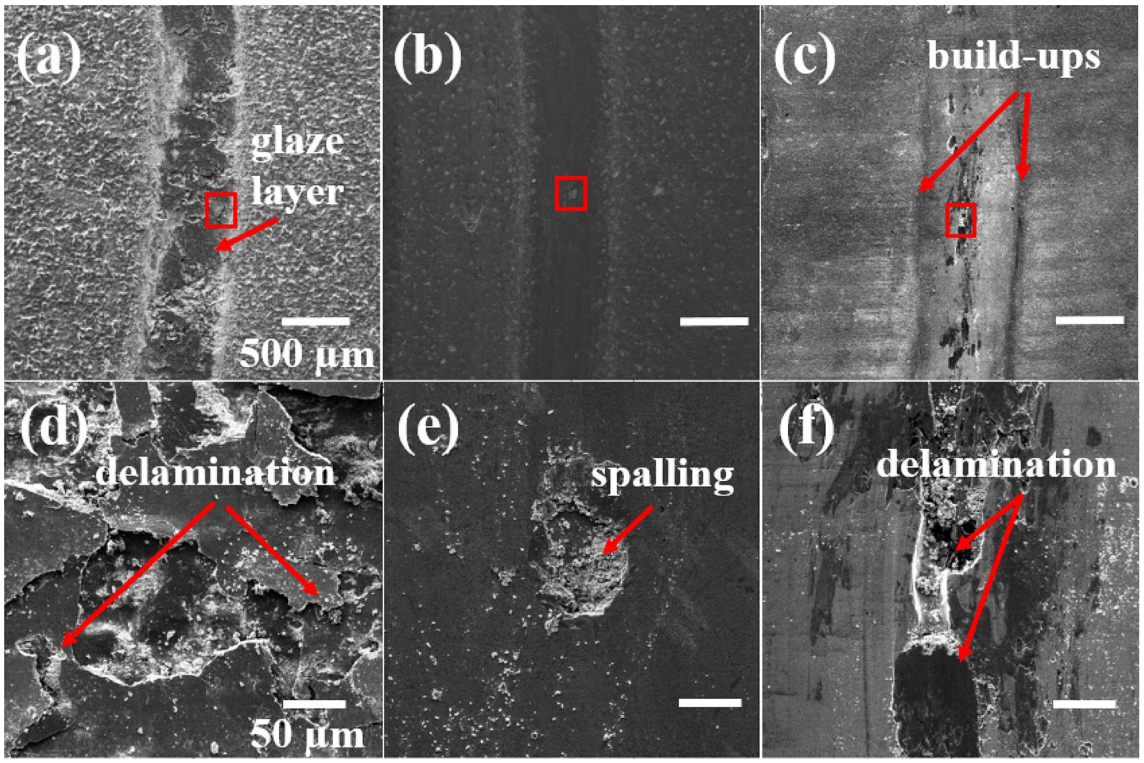


**Fig. 9** SEM images of the wear tracks on the disks tested at 450 °C at different magnifications. **a, d** CrC coating; **b, e** boronized coating; **c, f** Ni–P coating. Scale bars show the same length in each row. Small squares in **a**, **b**, and **c** depict the locations of **d**, **e,** and **f** respectively

High adhesive force between nickel and other metallic surfaces could result in increase of adhesive wear (Fig. 9f).

SEM images of the contact surface of the balls used as countersurface against CrC, boronized nickel alloy, and Ni–P coatings at 450 °C are shown in Fig. 10. The first major difference is the absence of any measurable wear on the balls, as compared to the balls used against the same coatings at RT. WC balls maintains its hardness at 450 °C which is approximately 1500 HK [52]. Figure 10d–f depict magnified views of the contact surface of the balls. While Fig. 10a shows an intact surface without much oxide transfer, magnified view in Fig. 10d reveals small particles which could be transferred from the CrC coating. Figure 10b depicts patchy transfer of oxide layers and wear debris to the ball slid against the boronized. A clear presentation of an oxide flake is provided in Fig. 10e. Such material transfer from the oxidized coating to the countersurface could render the tribocontact to an oxide-on-oxide sliding, provided adequate bonding between oxide and the substrates. This film transfer could help reduce the COF due to lower shear force required for sliding of such oxides as well as protecting the surface and restraining the wear by providing protection to the surface. Strips of oxide material are visible on ball used against the Ni–P coating, as shown in Fig. 10c, however further magnification reveals a loose attachment of the particles and flakes on the surface of the WC ball, which would not be effective especially regarding their scarcity on the surface. One could see the influence of such material transfer on the wear rate of the boronized nickel alloy.

In summary, the surfaces that could generate a uniform and strongly adhered oxidized layer experience lower wear and friction at higher temperatures. In contrast, at RT the surface topography and the mechanical properties (especially hardness) govern the wear and friction mechanisms.

### 3.4 EDX Analysis

To perform EDX analysis, a Tescan (LYRA-3 Model) FIB-SEM was used. The obtained spectra were analyzed with the Oxford EDX software package, INCA. Before each test, energy calibration was conducted using the standard copper tape, where applicable. To achieve a reliable representation of the chemical composition for each sample, energy spectra were collected over at least four different areas. Mean and the standard deviation of the obtained elemental compositions were used as average and error bars in the following figures. The acceleration voltage used for the CrC and Ni–P coatings was 20 kV. Samples which have light element(s) in their chemical composition, such as boron, present a special challenge on the EDX technique. Normally higher accelerating voltages result in an overestimation of the boron atomic composition, however this effect may be minimal

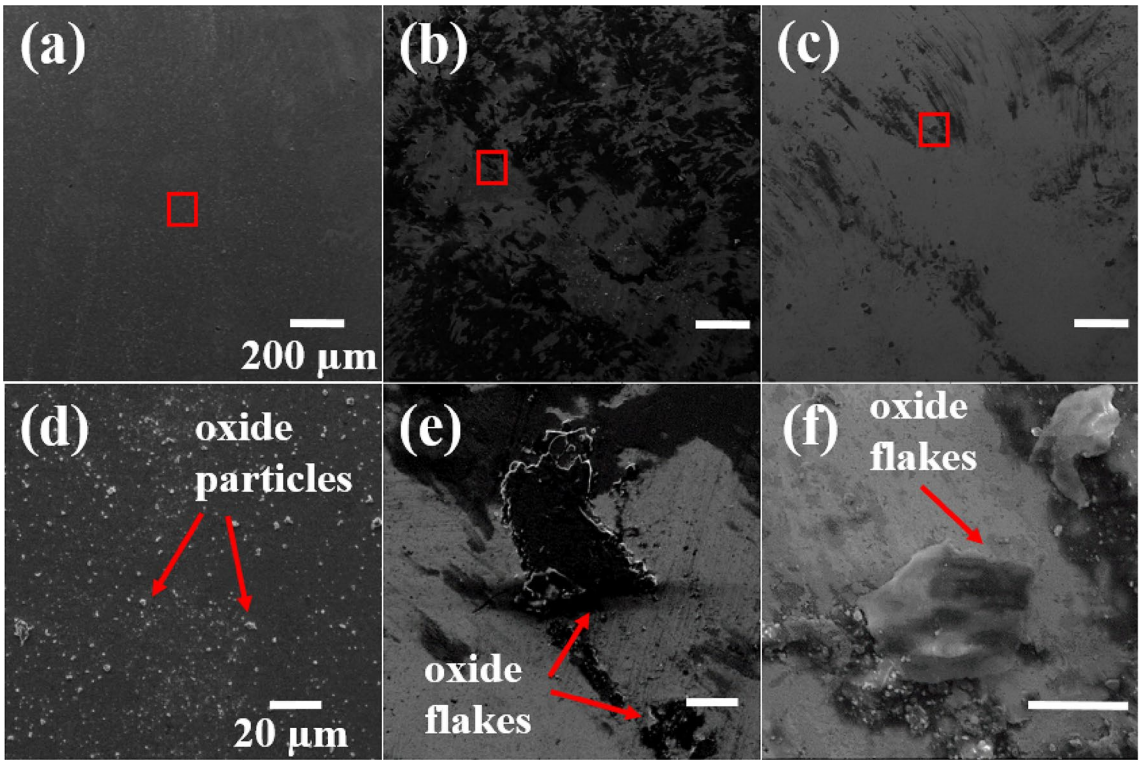


**Fig. 10** SEM images of the contact site on the balls tested at 450 °C at different magnifications: **a, d** CrC coating; **b, e** boronized coating; **c, f** Ni–P coating. Scale bars show the same length in each row. Small squares in **a**, **b**, and **c** depict the locations of **d**, **e,** and **f** respectively

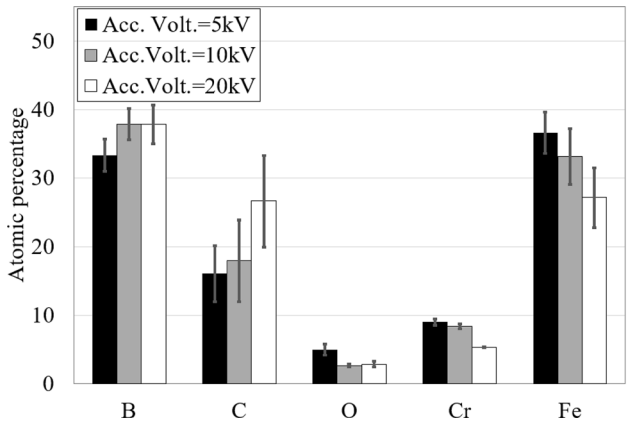


**Fig. 11** Effect of EDX acceleration voltage on the obtained atomic percentage of untested boronized nickel alloy coating

for high-boron content samples and could be minimized by optimizing the acceleration voltage. Thus, for the boronized nickel alloy coating a parametric study on the effect of the accelerating voltage on the detected values was conducted. Figure 11 depicts the obtained chemical compositions for the untested boronized nickel alloy sample obtained at different acceleration voltages: boron atomic percentage did not differ dramatically at an acceleration voltage of 5 kV when compared to 10 and 20 kV, and one could observe that they are quite comparable within the margin of uncertainty. Other elements such as iron and chromium may be affected more meaningfully at lower acceleration voltages. To avoid compromising the precise detection of atomic composition of other relatively heavier elements such as iron, chromium, tungsten, and cobalt as transferred materials, acceleration voltage of 10 kV was selected for the boronized coating. As a precautionary approach, the values of the detected elements reported only if the measured average value was more than one percent and three times higher than the standard deviation of the corresponding measurement.

Figures 12, 13, 14 present normalized elemental composition results obtained from EDX analyses conducted on the untested as well as tested surface coatings at different temperatures. The results help verify the previous discussion regarding the intensity of oxidation, material transfer, and changes in surface material compositions at different temperatures. For reference, the atomic percentages of the untested tungsten carbide balls, also obtained from EDX are: Tungsten: $57 \pm 5\%$, Carbon $33 \pm 3\%$, and Cobalt: $10 \pm 2\%$.

Figure 12 shows the average atomic percentages of chromium, carbon, iron, oxygen, cobalt, and tungsten elements on the wear track of the disks used in the experiments conducted with the CrC coatings. The obtained data at RT indicate similar elemental composition of the coating before and after the tests, which suggest an almost purely physical

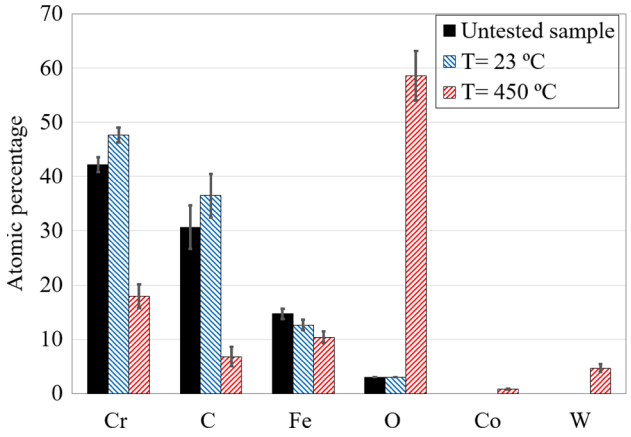


**Fig. 12** EDX elemental atomic percentages measured inside the wear tracks after tribo-testing at RT (23 °C) and 450 °C: CrC coating

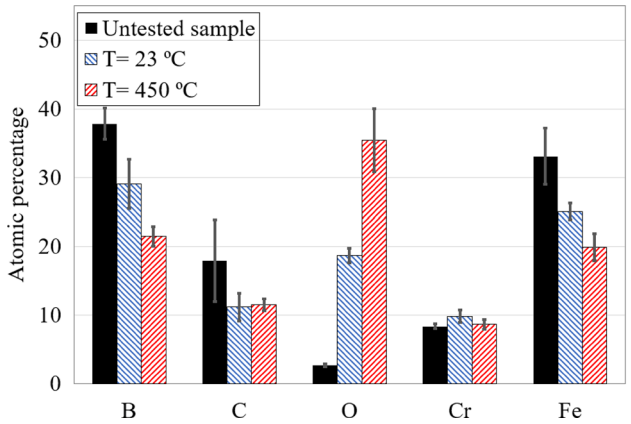


**Fig. 13** EDX elemental atomic percentages measured inside the wear tracks after tribo-testing at RT (23 °C) and 450 °C: boronized nickel alloy coating

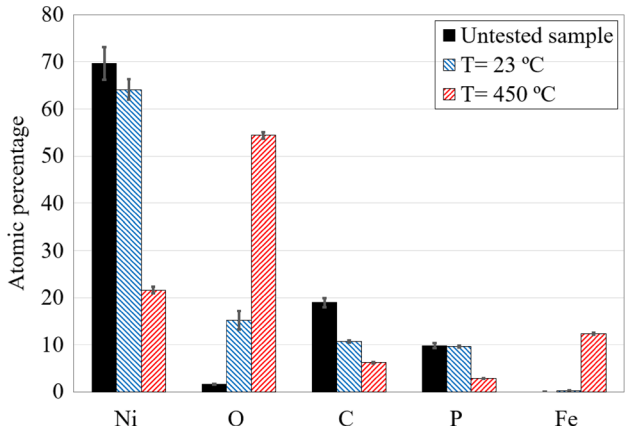


**Fig. 14** EDX elemental atomic percentages measured inside the wear tracks after tribo-testing at RT (23 °C) and 450 °C: Ni–P coating

tribo-behavior for the tests conducted at RT. Thus, explaining the changes in contacts at RT by referring to physical phenomena, such as adhesion/abrasion is justified. However, one can observe the diminishing of carbon and chromium at the elevated tribo-testing temperature. Both elements are the backbone of this coating structural skeleton. The transition of CrC polishing wear rate at RT to a substantial wear rate at 450 °C is because of degradation of these two elements possibly through oxidation reactions. Chromium oxide ($Cr_2O_3$) is a protective oxide [53] when forms uniformly and can adhere to the coating. In this case, it was fully developed and formed a glaze layer at 450 °C. Sudden increase of oxygen along with reduction of chromium could signify high production of chromium oxide. As shown, untested chromium carbide does not have any cobalt or tungsten constituents, thus small percentage of cobalt and tungsten on the coating surface represent the material transfer from the ball. Such material transfer was observed in the SEM images as well, and can change the dynamics of the contact. The oxidation process of tungsten and tungsten carbide was thoroughly investigated at RT to elevated temperatures [54], and weakening of the bonding was reported in tungsten and tungsten carbide with increasing temperature. This could justify the emergence of tungsten content at 450 °C.

EDX results of the boronized nickel alloy experiments are shown in Fig. 13. The boron content reduces slightly at RT test wear track, however, it shows notable reduction at 450 °C test wear track. It is known that the content of the boron decreases as deeper layers of boronized surfaces are penetrated [55]. Reduction in boron content correlates with the penetration depth of the wear tracks. A higher oxygen level on the RT sample is observed, compared to the untested sample, which implies moderate oxidation of the surface due to frictional heat generation and high contact pressure. Elevating the temperature to 450 °C results in higher oxidation of the surface which is clear from higher oxygen content. Iron and boron as the main elements of the boronizing coating follow similar trends, which was justified by the penetration in the coating. Chromium and carbon content do not experience significant changes within the margin of uncertainty.

Figure 14 shows the normalized atomic percentages of the constituents of Ni–P coatings tribotested at different temperatures. Increase in oxygen and iron percentages is concurrent with, and could be justified by, a decrease in the nickel content. A sharp increase in the oxidation is visible at 450 °C, however, the coating oxidation starts at RT which is due to very high frictional heat generation at the contact. The EDX analysis shows considerable amount of phosphorous that diminishes as the temperature increases. Iron content also reveals penetration of the coating at 450 °C knowing that the substrate is rich in iron. One can correlate the increase in the wear rate of Ni–P coating and the decrease in

its nickel content. Several other studies have investigated the critical role of nickel in increasing hardness and providing corrosion protection for tribological applications especially at elevated temperatures [48, 56].

## 4 Conclusion

The tribological properties and behavior of three coatings, namely CrC, Ni–P, boronized nickel alloy and their substrate, a Ni-resist alloy were investigated. Nanomechanical properties of the boronized and Ni–P coatings were obtained at RT, 200 °C, and 400 °C. Using a specialized tribometer, in-situ friction was measured and the corresponding wear rates were estimated at RT (23 °C) and 450 °C. Detailed analyses of the resultant wear tracks using profilometry, SEM and EDX techniques were carried out, resulting in the following conclusions:

- Both boronized nickel alloy and CrC coatings exhibited reasonably low wear rates at elevated temperature; the boronized coating showed superior wear performance for the tested temperature range. Ni–P coating was almost penetrated during high temperature test and deemed as not suitable for high temperature applications under present study conditions;
- Smooth Ni–P coating exhibited the highest COF, while the rough surface of CrC yielded lower COF at RT tests;
- COF for all coatings followed a decreasing trend with increasing temperature. This was due to the generation of stable oxidation layers with lower shear resistance and potentially material transfer between contacting surfaces. In addition, topographical changes in the contact region as well as changes in mechanical properties at elevated temperatures contributed to the results;
- 3D Surface topography and mechanical properties of the surfaces, particularly hardness were obtained using instrumented nanoindentation technique. Both properties play a critical role in low temperature wear and friction behaviors, while at elevated temperatures their importance is balanced by the chemical composition of the surface and the generated oxides;
- EDX analyses revealed the significance of oxides presence that is correlated to the tribological behavior of the coatings such as reduction in COF. In addition, material transfer from the sliding surface could alleviate the wear rates which was shown by the results in this study;
- Based on this study, it is possible to use boronized nickel alloy at elevated (up to 450 °C) tribological applications, where the COF is sufficiently low (i.e., 0.6) and stable, and the wear rate is low; and
- Friction and wear mechanisms of the coatings at elevated temperatures depend strongly on the changes in the mechanical properties of the tribopairs, and the properties of the generated oxides.

**Acknowledgements** This research work was supported in part by the Turbomachinery Research Consortium, an organization of major turbomachinery developers and users who have joined with the Turbomachinery Laboratory at Texas A&M University to find answers to important questions about turbomachinery performance and reliability.

### Compliance with Ethical Standards

**Conflict of interest** The authors declare that they have no conflict of interest.

## References

1. K. Homlberg, A. Matthews, Coating tribology, properties, techniques and applications in surface engineering, Tribol. Ser. **28** (1994)
2. Xu, Z., Shi, X., Zhang, Q., Zhai, W., Li, X., Yao, J., Song, S., Chen, L., Xiao, Y., Zhu, Q.: Wear and friction of TiAl matrix self-lubricating composites against $Si_3N_4$ in air at room and elevated temperatures. Tribol. Trans. **57**, 1017–1027 (2014). https://doi.org/10.1080/10402004.2014.931497
3. Blau, P.J., Erdman, D.L., Ohriner, E., Jolly, B.C.: High-temperature galling characteristics of ti-6AL-4 V with and without surface treatments. Tribol. Trans. **54**, 192–200 (2011). https://doi.org/10.1080/10402004.2010.534837
4. Holmberg, K., Mathews, A.: Coatings tribology: a concept, critical aspects and future directions. Thin Solid Films **253**, 173–178 (1994). https://doi.org/10.1016/0040-6090(94)90315-8
5. Prasad, S.V., McDevitt, N.T., Zabinski, J.S.: Tribology of tungsten disulfide-nanocrystalline zinc oxide adaptive lubricant films from ambient to 500°C. Wear **237**, 186–196 (2000). https://doi.org/10.1016/S0043-1648(99)00329-4
6. Gulbiński, W., Suszko, T., Sienicki, W., Warcholiński, B.: Tribological properties of silver-and copper-doped transition metal oxide coatings. Wear **254**, 129–135 (2003)
7. Medvedovski, E., Jiang, J.R., Robertson, M.: Tribological properties of boride based thermal diffusion coatings. Adv. Appl. Ceram. **113**, 427–437 (2014). https://doi.org/10.1179/1743676114Y.0000000175
8. Takács, G.: Electrical submersible pumps manual: design, operations, and maintenance. Gulf Professional Pub./Elsevier, Houston (2009)
9. Lee, L., Behera, P., Sriraman, K.R., Chromik, R.R.: The effect of contact stress on the sliding wear behaviour of Zn-Ni electrodeposited coatings. Wear **400–401**, 82–92 (2018). https://doi.org/10.1016/J.WEAR.2017.12.018
10. Abourayak, K., Fayeulle, S., Vincent, L., Ribeiro, C., Cavaleiro, A., Vieira, M.T.: Tribological behaviour at elevated temperatures of thin physical vapour deposited coatings. Surf. Coatings Technol. **80**, 171–175 (1996)
11. Fu, Y., Li, H., Ji, L., Liu, X., He, N., Zhou, H., Chen, J.: Preparation and high-temperature tribological properties of CrAlVYN-Ag nanocomposite coatings. Mater. Manuf. Process. **32**, 409–415 (2017). https://doi.org/10.1080/10426914.2016.1176189
12. Radil, K., DellaCorte, C.: The performance of PS400 subjected to sliding contact at temperatures from 260 to 927°C. Tribol. Trans. **60**, 957–964 (2017). https://doi.org/10.1080/10402004.2016.1231357

13. Li, J., Xiong, D.: Tribological behavior of graphite-containing nickel-based composite as function of temperature, load and counterface. Wear **266**, 360–367 (2009). https://doi.org/10.1016/J.WEAR.2008.06.020
14. Hu, E., Hu, X., Liu, T., Fang, L., Dearn, K.D., Xu, H.: The role of soot particles in the tribological behavior of engine lubricating oils. Wear **304**, 152–161 (2013). https://doi.org/10.1016/j.wear.2013.05.002
15. Li, J.L., Xiong, D.S.: Tribological properties of nickel-based self-lubricating composite at elevated temperature and counterface material selection. Wear **265**, 533–539 (2008). https://doi.org/10.1016/J.WEAR.2007.09.005
16. Zhen, J., Li, F., Zhu, S., Ma, J., Qiao, Z., Liu, W., Yang, J.: Friction and wear behavior of nickel-alloy-based high temperature self-lubricating composites against Si3N4 and Inconel 718. Tribol. Int. **75**, 1–9 (2014). https://doi.org/10.1016/J.TRIBOINT.2014.03.005
17. Polcar, T., Cvrček, L., Široký, P., Novák, R.: Tribological characteristics of CrCN coatings at elevated temperature. Vacuum **80**, 113–116 (2005). https://doi.org/10.1016/j.vacuum.2005.07.033
18. Singla, Y.K., Dwivedi, D.K., Arora, N.: On the modeling of dry sliding adhesive wear parameters of vanadium additive iron-based alloys at elevated temperatures. Surf. Coatings Technol. **283**, 223–233 (2015). https://doi.org/10.1016/j.surfcoat.2015.10.078
19. Polychronopoulou, K., Demas, N.G., Gibson, P.N., Rebholz, C., Polycarpou, A.A.: Effect of Cu content on the structure, and performance of substoichiometric Cr-N coatings. Tribol. Lett. **38**, 57–68 (2010). https://doi.org/10.1007/s11249-009-9572-x
20. Hardell, J., Prakash, B.: Tribological performance of surface engineered tool steel at elevated temperatures. Int. J. Refract. Met. Hard Mater. **28**, 106–114 (2010). https://doi.org/10.1016/j.ijrmhm.2009.07.009
21. Taktak, S.: Tribological behaviour of borided bearing steels at elevated temperatures. Surf. Coatings Technol. **201**, 2230–2239 (2006). https://doi.org/10.1016/j.surfcoat.2006.03.032
22. Solzak, T.A., Polycarpou, A.A.: Tribology of hard protective coatings under realistic operating conditions for use in oilless piston-type and swash-plate compressors. Tribol. Trans. **53**, 319–328 (2010). https://doi.org/10.1080/10402000903283300
23. Acchar, W., Gomes, U.U., Kaysser, W.A., Goring, J.: Strength degradation of a tungsten carbide-cobalt composite at elevated temperatures. Mater. Charact. **41**, 27–32 (1999)
24. Gheisari, R., Polycarpou, A.A.: Three-body abrasive wear of hard coatings: effects of hardness and roughness. Thin Solid Films **666**, 66–75 (2018). https://doi.org/10.1016/J.TSF.2018.07.052
25. Ranganatha, S., Venkatesha, T.V., Vathsala, K.: Development of high performance electroless Ni–P–HNT composite coatings. Appl. Surf. Sci. **263**, 149–156 (2012). https://doi.org/10.1016/J.APSUSC.2012.09.020
26. Novák, M., Vojtěch, D., Vítů, T.: Influence of heat treatment on tribological properties of electroless Ni–P and Ni–P–Al2O3 coatings on Al–Si casting alloy. Appl. Surf. Sci. **256**, 2956–2960 (2010). https://doi.org/10.1016/J.APSUSC.2009.11.057
27. Yoon, J., Jee, Y., Lee, S.: Plasma paste boronizing treatment of the stainless steel AISI 304. Surf. Coatings Technol. **112**, 71–75 (1999). https://doi.org/10.1016/S0257-8972(98)00743-9
28. Tabur, M., Izciler, M., Gul, F., Karacan, I.: Abrasive wear behavior of boronized AISI 8620 steel. Wear **266**, 1106–1112 (2009). https://doi.org/10.1016/J.WEAR.2009.03.006
29. Sen, U.: Friction and wear properties of thermo-reactive diffusion coatings against titanium nitride coated steels. Mater. Des. **26**, 167–174 (2005). https://doi.org/10.1016/j.matdes.2004.05.010
30. Chen, F.S., Lee, P.Y., Yeh, M.C.: Thermal reactive deposition coating of chromium carbide on die steel in a fluidized bed furnace. Mater. Chem. Phys. **53**, 19–27 (1998). https://doi.org/10.1016/S0254-0584(97)02048-8
31. Zikin, A., Hussainova, I., Katsich, C., Badisch, E., Tomastik, C.: Advanced chromium carbide-based hardfacings. Surf. Coatings Technol. **206**, 4270–4278 (2012). https://doi.org/10.1016/J.SURFCOAT.2012.04.039
32. Oliver, W.C., Pharr, G.M.: An improved technique for determining hardness and elastic modulus using load and displacement sensing indentation experiments. J. Mater. Res. **7**, 1564–1583 (1992). https://doi.org/10.1557/JMR.1992.1564
33. Lan, P., Zhang, Y., Dai, W., Polycarpou, A.A.: A phenomenological elevated temperature friction model for viscoelastic polymer coatings based on nanoindentation. Tribol. Int. **119**, 299–307 (2018). https://doi.org/10.1016/J.TRIBOINT.2017.11.009
34. Engqvist, H., Wiklund, U.: Mapping of mechanical properties of WC-Co using nanoindentation. Tribol. Lett. **8**, 147–152 (2000). https://doi.org/10.1023/A:1019143419984
35. Duszová, A., Halgaš, R., Bľanda, M., Hvizdoš, P., Lofaj, F., Dusza, J., Morgiel, J.: Nanoindentation of WC–Co hardmetals. J. Eur. Ceram. Soc. **33**, 2227–2232 (2013). https://doi.org/10.1016/J.JEURCERAMSOC.2012.12.018
36. Gee, M.G., Roebuck, B., Lindahl, P., Andren, H.-O.: Constituent phase nanoindentation of WC/Co and Ti(C, N) hard metals. Mater. Sci. Eng., A **209**, 128–136 (1996). https://doi.org/10.1016/0921-5093(95)10099-7
37. Wood, R.J.K.: Tribology of thermal sprayed WC–Co coatings. Int. J. Refract. Met. Hard Mater. **28**, 82–94 (2010). https://doi.org/10.1016/J.IJRMHM.2009.07.011
38. Kundu, S., Das, S.K., Sahoo, P.: Influence of load and temperature on tribological behaviour of electroless Ni-P deposits. IOP Conf. Ser. Mater. Sci. Eng. **149**, 12046 (2016)
39. Gök, M.S., Küçük, Y., Erdoğan, A., Öge, M., Kanca, E., Günen, A.: Dry sliding wear behavior of borided hot-work tool steel at elevated temperatures. Surf. Coatings Technol. **328**, 54–62 (2017). https://doi.org/10.1016/j.surfcoat.2017.08.008
40. Li, J., Xiong, D., Wu, H., Dai, J., Cui, T.: Tribological properties of molybdenized silver-containing nickel base alloy at elevated temperatures. Tribol. Int. **42**, 1722–1729 (2009). https://doi.org/10.1016/j.triboint.2008.12.004
41. Geng, Z., Duan, D., Hou, S., Li, S.: Tribological behavior of WC-12Co air plasma-sprayed coating at elevated temperatures. Tribol. Trans. **59**, 55–61 (2016). https://doi.org/10.1080/10402004.2015.1068423
42. Kundu, S., Das, S.K., Sahoo, P.: Influence of load and temperature on tribological behaviour of electroless Ni-P deposits. IOP Conf. Ser. Mater. Sci. Eng. **149**, 012046 (2016). https://doi.org/10.1088/1757-899x/149/1/012046
43. Lan, P., Meyer, J.L., Vaezian, B., Polycarpou, A.A.: Advanced polymeric coatings for tilting pad bearings with application in the oil and gas industry. Wear **354–355**, 10–20 (2016). https://doi.org/10.1016/j.wear.2016.02.013
44. H.O. Pierson, Handbook of refractory carbides and nitrides: properties, characteristics, processing and applications, William Andrew, 1996
45. León, O., Staia, M., Hintermann, H.: High temperature wear of an electroless Ni–P–BN (h) composite coating. Surf. Coatings Technol. **163–164**, 578–584 (2003). https://doi.org/10.1016/S0257-8972(02)00663-1
46. Lin, K., Lai, P.: The Crystallization of an Electroless Ni-P Deposit. J. Electrochem. Soc. **136**, 3803–3809 (1989). https://doi.org/10.1149/1.2096552
47. Parker, K.: Effects of heat treatment on the properties of electroless nickel deposits. Plat. Surf. Finish. **68**, 71–77 (1981)
48. Palaniappa, M., Seshadri, S.K.: Friction and wear behavior of electroless Ni–P and Ni–W–P alloy coatings. Wear **265**, 735–740 (2008). https://doi.org/10.1016/j.wear.2008.01.002

49. Takeuchi, E., Fujii, K., Katagiri, T.: Sliding wear characteristics of gas boronized steel. Wear **55**, 121–130 (1979). https://doi.org/10.1016/0043-1648(79)90184-4
50. Sen, S., Sen, U., Bindal, C.: Tribological properties of oxidised boride coatings grown on AISI 4140 steel. Mater. Lett. **60**, 3481–3486 (2006). https://doi.org/10.1016/J.MATLET.2006.03.036
51. Bindal, C., Erdemir, A.: Ultralow friction behavior of borided steel surfaces after flash annealing. Appl. Phys. Lett. **923**, 923 (1995). https://doi.org/10.1063/1.116232
52. Staia, M.H., D'Alessandria, M., Quinto, D.T., Roudet, F., Marsal Astort, M.: High-temperature tribological characterization of commercial TiAlN coatings. J. Phys. Condens. Matter. **18**, S1727 (2006). https://doi.org/10.1088/0953-8984/18/32/s04
53. Wang, D.-Y., Weng, K.-W., Chang, C.-L., Ho, W.-Y.: Synthesis of Cr3C2 coatings for tribological applications. Surf. Coatings Technol. **120–121**, 622–628 (1999). https://doi.org/10.1016/S0257-8972(99)00430-2
54. Casas, B., Ramis, X., Anglada, M., Salla, J., Llanes, L.: Oxidation-induced strength degradation of WC–Co hardmetals. Int. J. Refract. Met. Hard Mater. **19**, 303–309 (2001). https://doi.org/10.1016/S0263-4368(01)00033-6
55. Asthana, P., Liang, H., Usta, M., Ucisik, A.H.: Wear and surface characterization of boronized pure iron. J. Tribol. **129**, 1 (2007). https://doi.org/10.1115/1.2401211
56. Balaraju, J.N., Sankara Narayanan, T.S.N., Seshadri, S.K.: Electroless Ni–P composite coatings. J. Appl. Electrochem. **33**, 807–816 (2003). https://doi.org/10.1023/a:1025572410205